The Astrophysical Journal, 599:1418–1425, 2003 December 20


# TETHER-CUTTING ENERGETICS OF A SOLAR QUIET-REGION PROMINENCE ERUPTION

Alphonse C. Sterling[1, 2] and Ronald L. Moore
NASA Marshall Space Flight Center, SD50/Space Science Department, Huntsville, AL 35812;
asterling@solar.stanford.edu, ron.moore@nasa.gov
*Received 2003 May 31; accepted 2003 August 19*

## ABSTRACT

We study the morphology and energetics of a slowly evolving quiet-region solar prominence eruption occurring on 1999 February 8–9 in the solar north polar crown region, using soft X-ray data from the soft X-ray telescope (SXT) on *Yohkoh* and Fe xv EUV 284 Å data from the EUV Imaging Telescope (EIT) on the *Solar and Heliospheric Observatory* (*SOHO*). After rising at $\approx$1 km s$^{-1}$ for about six hours, the prominence accelerates to a velocity of $\approx$10 km s$^{-1}$, leaving behind EUV and soft X-ray loop arcades of a weak flare in its source region. Intensity dimmings occur in the eruption region cospatially in EUV and soft X-rays, indicating that the dimmings result from a depletion of material. Over the first two hours of the prominence's rapid rise, flarelike brightenings occur beneath the rising prominence that might correspond to "tether-cutting" magnetic reconnection. These brightenings have heating requirements of up to $\sim 10^{28}$–$10^{29}$ ergs, and this is comparable to the mechanical energy required for the rising prominence over the same time period. If the ratio of mechanical energy to heating energy remains constant through the early phase of the eruption, then we infer that coronal signatures for the tether cutting may not be apparent at or shortly after the start of the fast phase in this or similar low-energy eruptions, since the plasma-heating energy levels would not exceed that of the background corona.

*Subject headings:* Sun: corona — Sun: flares — Sun: UV radiation
*On-line material:* color figures

## 1. INTRODUCTION

Broadly speaking, solar filament and prominence eruptions are of two different types: active-region eruptions and quiet-region eruptions. Each type has its own characteristics (e.g., Zirin 1988), but both can be associated with brightenings, or "flaring," in soft X-rays, with the active-region flares often brighter than the quiet-region flares. Among the other differences between the two types are the magnetic environment in which they occur, with the quiet regions having substantially weaker field strengths than the active regions, and the rates at which their evolutions progress, with the quiet-region events occurring on much longer timescales than the active-region events. We can make the assumptions that both types of eruptions are aspects of a more general magnetic eruption process and that the mechanism driving these eruptions is the same in the two cases, only differing on scales related to the respective magnetic field strengths. In that case, we can study the time evolution of eruptions in greater detail by looking at the slower evolving quiet-region events. We have recently done just this to try to understand the energy release mechanism for a filament eruption that occurred on 1999 April 18 (Sterling, Moore, & Thompson 2001b; Sterling & Moore 2004). Our primary data for that event were EUV images in 195 Å Fe xii from EIT and soft X-ray images from SXT, along with magnetic field data.

Here we continue investigating slow eruptions by studying a quiet-region prominence eruption that occurred on 1999 February 8–9, using SXT and EIT data. In this case, our highest cadence EIT data are from the 284 Å Fe xv filter. The 284 Å images often show cool features such as prominences in absorption more strikingly than do the 195 Å images while concurrently showing hotter regions of the corona than do the 195 Å images. We investigate the coronal characteristics of this eruption and compare them with findings from related studies.

A second aim of this current work is to consider the energetics of the 1999 February 8–9 erupting prominence system in order to learn about possible limitations of using observations of low-energy events to investigate eruption mechanisms. Several proposed mechanisms predict that magnetic fields below an erupting prominence reconnect, releasing stored energy as a solar flare. This reconnection is sometimes referred to as "tether cutting," since in some views the magnetic fields involved in the reconnection are like tethers holding down the prominence. Work of, e.g., Moore & LaBonte (1980), Sturrock (1989), and Moore et al. (2001), proposes that tether cutting is the agent responsible for the primary energy release that triggers eruptions (we refer to this as the "tether-cutting model"). Other mechanisms, however, can also lead to tether cutting as a secondary consequence of a different eruption mechanism, where the timings of the flare brightening relative to the fast-eruption onset can differ depending on the mechanism. In attempts to understand what triggers eruptions, we recently considered this timing question for fast eruptions (e.g., Sterling et al. 2001a) and also for slow eruptions (Sterling et al. 2001b and Sterling & Moore 2004, who examined the above-mentioned 1999 April 18 slow eruption.)

Our aim in studying the prominence energetics here is not to deal with the eruption trigger question directly. Instead, we investigate the more general question of the expected observational detectability of tether-cutting reconnection accompanying fast-eruption onset, independent of whether

[1] United Applied Technologies, Inc., 11506 Gilleland Drive, Huntsville, AL 35803.
[2] Current address: Institute of Space and Astronautical Science, Yoshinodai 3-1-1, Sagamihara, Kanagawa 229-8510, Japan.

the tether cutting is the trigger or a consequence of the eruption. This more general question is important, because for low-energy events, such as the one considered here, it is not obvious beforehand whether tether-cutting heating during early phases of eruptions is greater than that of the background atmosphere; if it is weaker than the background, then signatures of the reconnection will not be detectable early enough to use in checking model predictions. Results of this study will help to determine for which events it is appropriate to use timing analysis in future studies, to attempt to differentiate observationally between proposed eruption onset mechanisms.

## 2. INSTRUMENTATION AND DATA

EIT images the Sun with four EUV filters, along with a CCD detector with 2.″6 pixels. EIT has been operating in "CME watch" mode nearly continuously since early 1997, whereby it takes full-disk images in the same filter with a cadence of approximately 15 minutes. Most of the time these campaigns use the 195 Å Fe XII filter, but occasionally other filters are used. One such period was during 1999 February, when the 284 Å Fe XV filter was employed, and among those data we found the prominence eruption presented here. This filter is most sensitive to material emitting at about 2.0 MK. The *Solar and Heliospheric Observatory* (*SOHO*) is in a solar orbit at the L1 Lagrangian point and therefore is not subject to spacecraft night. Delaboudiniere et al. (1995) give a description of EIT.

SXT images the Sun in various operating modes and in several soft X-ray filters; they cover the approximate wavelength range 3–45 Å, resulting in sensitivity to plasmas at temperatures $\gtrsim 2$ MK. Here we use subfields of full-disk images, which have pixel resolution of 4.″9 or 9.″8. Our data have time cadence of typically 3–8 minutes, with longer gaps for spacecraft night. Tsuneta et al. (1991) give details of the SXT instrument.

Our prominence was anchored in the fields of the north polar crown and existed since at least 00:00 UT on 1999 February 7, when it was near the northeastern limb. It was stable until the start of its eruption late on 1999 February 8. Soft X-ray emissions from this event were weak; at most, there was an enhancement in the *GOES* satellite flux that might have been associated with this event at about a mid-B *GOES* class level, which was close to the background level for that time. Nonetheless, the eruption produced an arcade of loops in SXT and EIT images, suggesting that it was a typical ejective eruption (Moore et al. 2001).

## 3. OBSERVATIONS

Figure 1 shows EIT 284 Å images of the prominence around the time of eruption. During the period well before eruption (e.g., Fig. 1*a*), the top of the prominence appears to exchange material with a remote filament to the southeast, located at about (−800″, 400″). As eruption time approached (Fig. 1*b*), the prominence began to move upward and showed a more fragmentary structure. This fragmentation is more obvious when the eruption is further advanced (Fig. 1*c*). After the prominence is gone (Fig. 1*d*) an arcade of loops remains in the eruption source region. Between the first and last panels of Figure 1 substantial intensity dimming occurs in the region just west of the prominence's original location.

Figure 2 shows SXT AlMg images at times similar to those in Figure 1. There is no obvious manifestation of the prominence in soft X-rays in Figures 2*a* and 2*b*. Following eruption, however, a postflare arcade dominates the region (Figs. 2*c* and 2*d*).

Figure 3 marks various locations in the eruption region with boxes from which we define light curves. Figures 3*a* and 3*c*, respectively, show EIT and SXT images at the specified times, while Figures 3*b* and 3*d*, respectively, show EIT and SXT "percentage-difference images," in which an earlier image is subtracted from a later image and the result divided by the earlier image; such percentage difference images sometimes do better at reproducing contrasts than do straight "difference images" (Wills-Davey & Thompson 1999; Harra & Sterling 2003). Boxes 1 and 2 identify locations where we detect the earliest brightenings in EIT and SXT, and box 3 identifies a region of strong coronal dimming that we also see in both EIT and SXT.

Box 4 is from a location we believe to be relatively free from eruption-associated brightenings and dimmings in EIT (scattered light from a nearby active region contaminates the SXT image at this box location), which we use for reference; we place this box near the limb because of a known effect resulting in spurious dimmings near the east limb in solar rotation–corrected images. This artificial dimming, along with corresponding artificial brightening near the west limb, results from a combination of the rotation-correction procedure and the limb-brightening effect and becomes more pronounced as the time between the images being differenced increases (Sterling & Moore 2004). These false dimmings and brightenings occur in both EIT and SXT, but Sterling & Moore (2004) found them to be weaker in SXT than in EIT (although they only considered EIT 195 Å images), probably because limb brightening is weaker in the SXT images.

Figure 4 shows light curves from the boxed regions of Figure 3 for EIT and SXT; for each box, we summed the intensity in the original (i.e., nondifferenced) images over the entire box, divided by the number of pixels, and normalized the time to give the results per second. We also plot the trajectory of the prominence as a function of time, where we have measured the prominence's height relative to a weak intensity feature that appears to be stationary and that we can follow from frame to frame throughout the prominence's ascent; the bottom arrow in Figures 1*a* and 1*b* point out this feature. Identification of the top of the prominence was not always unique, especially during ascent, when the whole structure became more fragmented. In each image we selected two points, the lower of which appeared to be the top of the bulk of the prominence mass and the upper of which was near the highest extensions of the prominence; the uppermost two arrows in Figures 1*a* and 1*b* show our selections for those frames. In the Figure 4 trajectory we plot the mean of these two heights. Differences in these upper and lower estimates for the prominence height vary from about $5 \times 10^3$ to about $2.3 \times 10^4$ km, generally showing a weak increasing trend with time.

Instead of being smooth, the prominence's trajectory appears to change form around 22:30 UT, and we find that separately the two halves can be well fitted. In the plot of the prominence height (in units of $10^5$ km) in Figure 4, a fit combining a linear fit to 21 data points between 17:10:27 UT and 22:25:04 UT on February 8 and a quadratic fit for the

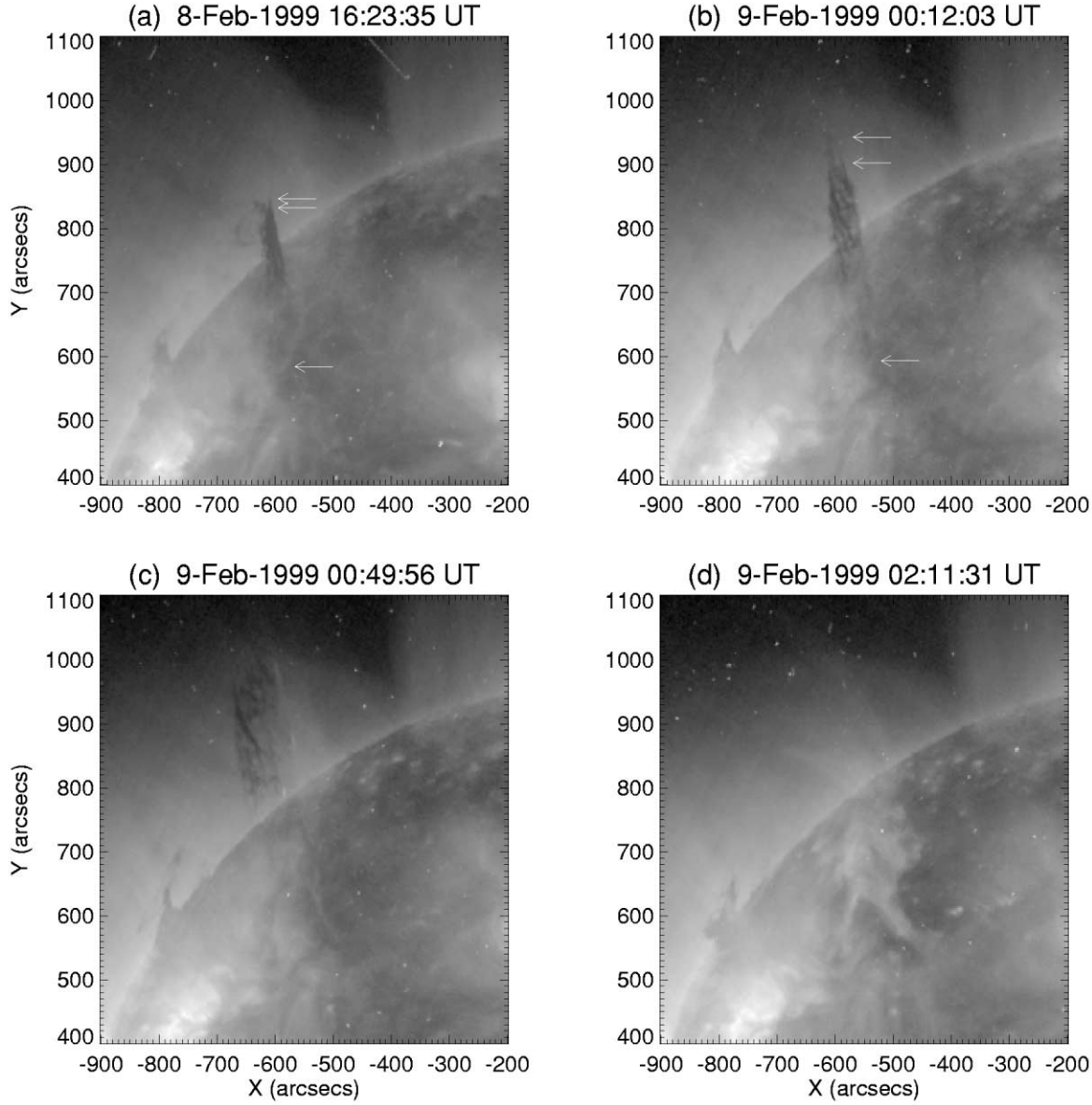


FIG. 1.—EIT 284 Å images of the prominence eruption in the northern solar polar crown region. In (*a*) and (*b*), the lowest arrow shows a weak feature we use to reference the distance the prominence moves as a function of time. The top two arrows give upper and lower bounds for our estimate of the location of the top of the prominence. East is left and north is toward the top in this and all other images in the paper. [*See the electronic edition of the Journal for a color version of this figure*.]

10 points between 22:25:04 UT February 8 and 00:49:56 UT February 9 gives a $\chi^2 = 0.06$ over the full range. In contrast, attempting to fit a single quadratic to the entire range of 31 points gives $\chi^2 = 0.3$, and thus, the evidence favors a two-stage path for the prominence's rise. Figure 4*b* shows the two-component (linear and quadratic) fits overplotted on the prominence trajectory. We could have tried a quadratic fit to the early points or a linear fit to the later points, but what we have done is sufficient to approximate the trajectory during the evolution. For the early portion the slope of the fitted line gives a velocity of 1.2 km $s^{-1}$, and for the later points the tangent to the fitted curve around 23:45 UT on February 8 gives a velocity of about 10.3 km $s^{-1}$. This two-stage ascent, with a period of acceleration, is similar to the filament eruption studied by Sterling et al. (2001b) and Sterling & Moore (2004), where the respective velocities were 1 and 16 km $s^{-1}$; we refer to these as pre- and posteruption velocities, respectively.

If we use our uppermost estimate for the prominence top rather than the mean value, the pre- and posteruption velocities are 1.4 and 10.3 km $s^{-1}$, respectively. Using our lowest estimate for the prominence top gives 1.1 km $s^{-1}$ and, once again, 10.3 km $s^{-1}$, respectively.

During the preeruption phase, the EIT box 3 light curve in Figure 4*a* shows a steady decrease with time. Yet, prior to about 22:00 UT, we are not sure whether this is true dimming or if it is the spurious dimming mentioned above and discussed by Sterling & Moore (2004). Our light curve from box 4 shows an example of what might be this spurious dimming, and the intensity decrease of the box 2 curve prior to about 0 UT may also be spurious. We do not know how this spurious

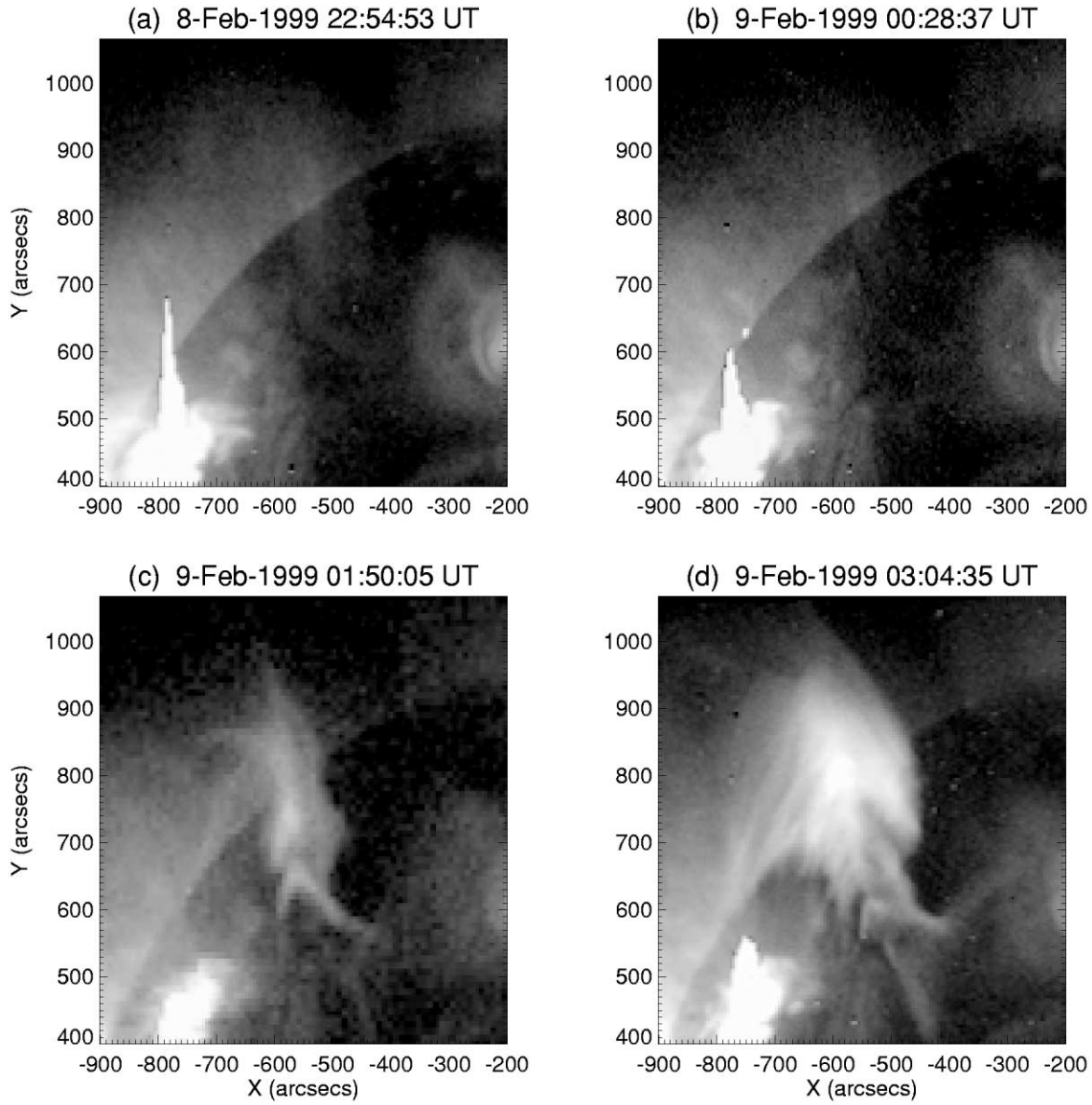


FIG. 2.—SXT AlMg images of the eruption region at four different times. [*See the electronic edition of the Journal for a color version of this figure.*]

dimming quantitatively depends on factors such as the initial intensity of the emitting features, so we do not attempt to correct for it here. We do not consider further any of the apparent dimmings prior to 22:00 UT. Anyhow, the principal dimmings (box 3) and brightenings (boxes 1 and 2) greatly exceed the magnitude of any possibly spurious dimmings suggested by box 4. We omit the curve for box 4 for SXT in Figure 4*b* because of the scattered light in the box from the active region; we expect these spurious intensities to be smaller than those of EIT, both because of the shorter time coverage in SXT and also because the effect in general seems to be weaker in SXT than EIT, as mentioned above and as found by Sterling & Moore (2004).

Prominent dimming begins in EIT near the onset of the prominence's eruption phase, just after 22:00 UT (cf. Fig. 3*b*), and we also see obvious SXT dimming from 00:05 UT. Figure 3*d* shows the SXT dimming from 00:29 UT, with an image from 22:54 UT subtracted; *Yohkoh* was in spacecraft night prior to 22:54 UT, but there is no substantial change in the difference image of Figure 3*d* if we subtract a prenight SXT image at 19:23 UT instead of the 22:54 UT image. In Figure 4, both EIT and SXT show brightening in the box 3 light curve from around 2:00 UT as the postflare arcade spreads into the region of that box.

## 4. ENERGETICS

From Figures 2*a*, 2*b*, and 3*d*, and from the box 1 curve in Figure 4*b*, we see that the soft X-ray emission from the expected tether-cutting reconnection region is very low at the time of the start of the prominence's fast-rise phase. One of our goals is to examine whether tether-cutting reconnection is expected to be observable at all at that time. As mentioned in § 1, several theories predict tether cutting to occur near the start of the eruption, and close examination of relative timings of tether-cutting brightenings and prominence motions can be a tool for differentiating between theories.

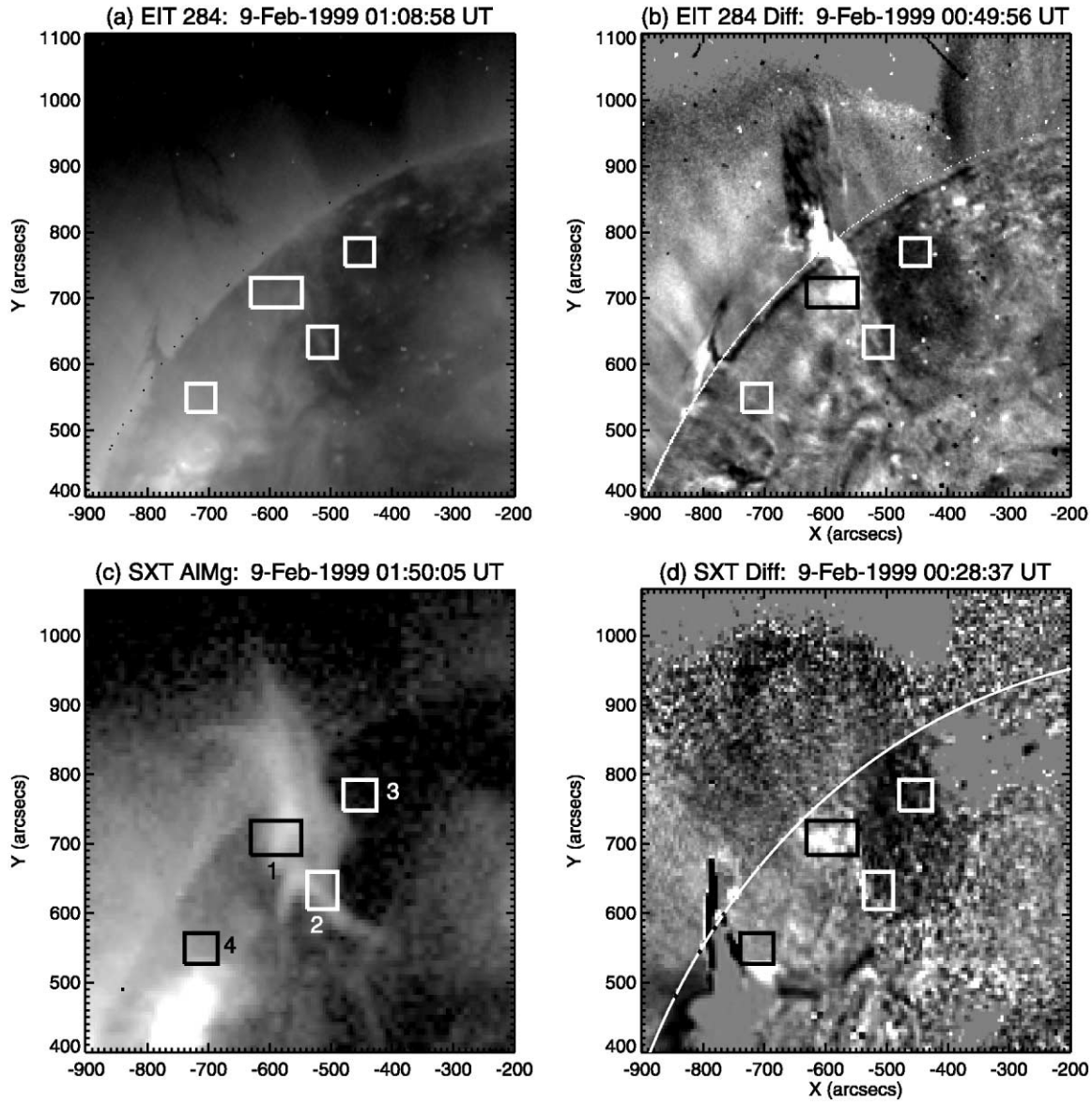


FIG. 3.—(*a*) and (*c*): Posteruption images in EIT 284 Å and SXT AlMg, respectively. (*b*) A percentage difference image in EIT 284 Å at the time given in the label, with the reference image from 1999 February 8, 16:23:35 UT. (*d*) SXT percentage difference image at the time given in the label and with reference image from 1999 February 8, 22:54:53 UT (Fig. 2*a* image). We corrected for differential solar rotation, with all images rotated to 03:30 UT 1999 February 9; this rotation was not applied to points beyond the limb and therefore caution is needed in interpreting off-disk features in these panels. This is most obvious in the difference images, where the time differences are greatest. Boxes labeled in (*c*) are used for creating light curves in Fig. 4.

Therefore, if, for example, some class of theories predicts strong tether cutting at the time of the start of rapid prominence motion, then our observations of weak intensity might rule out that class of theories.

In this section we make an educated guess at how energetic the tether cutting should be at the time of the rapid rise. We do this by calculating the energy associated with brightening in the reconnection region during a time when the brightenings are obvious and comparing it with the mechanical energy associated with the erupting prominence. We then make an assumption about how to extrapolate this result back to the time of eruption onset to see whether we would expect to see brightenings then.

First we estimate the amount of energy required for the prominence eruption, $E_{\rm prom}$, during the first hour of its rapid rise, roughly from 22:30 UT to 23:30 UT. This corresponds to the change over that period in the sum of the kinetic and potential energies,

$$E_{\rm prom} \approx \tfrac{1}{2} M(v_{\rm post}^2 - v_{\rm pre}^2) + Mg\Delta h \,, \qquad (1)$$

where we take $v_{\rm pre}$ and $v_{\rm post}$, the velocities before and after the period of rapid acceleration, to be $\approx$1 and 10 km s$^{-1}$, respectively, over which time the prominence's height increases by about $\Delta h \approx 2 \times 10^4$ km. For the mass, $M$, we assume a prominence density of $10^{10}$–$10^{11}$ cm$^{-3}$ (e.g., Schmahl & Hildner 1977; Rust et al. 1980), and we estimate the volume from the size of the prominence in Figure 1*a* or 1*b*. Its cross-sectional size is about $130'' \times 30''$, and if we take the length along the line-of-sight direction also to be $130''$ and assume a filling factor of 0.1, this gives $M \sim 10^{14}$–$10^{15}$ g. These numbers

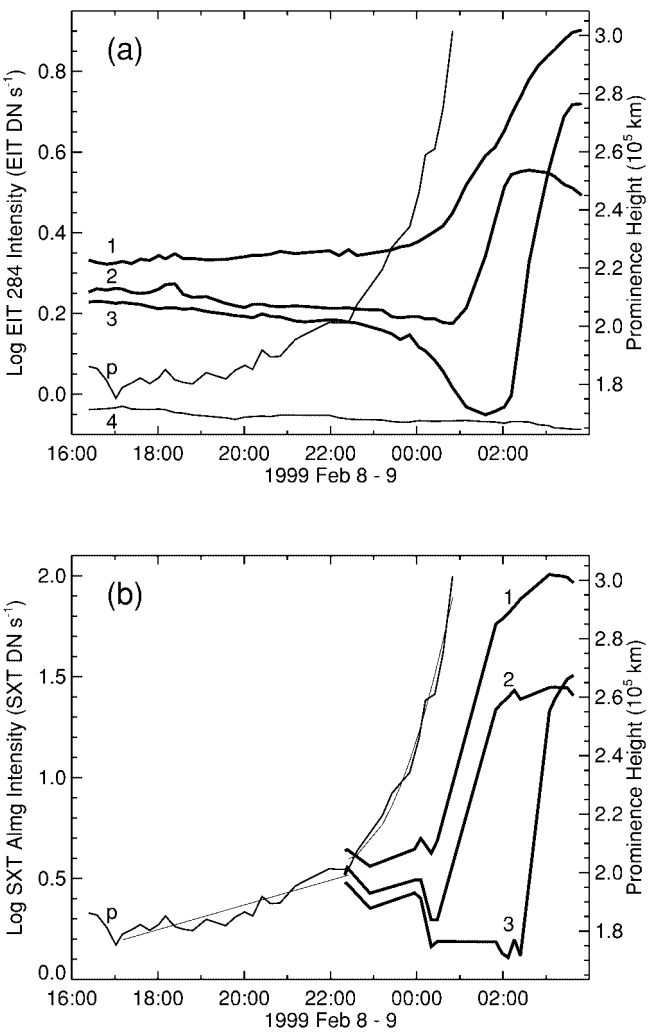


FIG. 4.—Light curves as functions of time of integrated and normalized (over time and spatial dimension) regions of boxes identified in Fig. 3 for (*a*) EIT 284 and (*b*) SXT AlMg rotation-corrected nondifferenced images, where numbers correspond to the box numbers of Fig. 3*c*. Overlaid in each panel is the trajectory, labeled "p," of the mean value of the top of the prominence. Thin lines in (*b*) are linear and quadratic (prior to and after 22:25 UT, respectively) fits to the prominence trajectory. We have shifted light curve 4 downward by one unit (i.e., a factor of 10) on the vertical axis for clarity.

indicate that the gravitational energy dominates the kinetic energy by 2 orders of magnitude, and

$$E_{\rm prom} \approx \Delta E_{\rm grav} \sim 10^{28}\text{–}10^{29} \text{ ergs} . \quad (2)$$

Next we estimate heating energy associated with tether-cutting reconnection. This is the sum of the radiated energy and the gain in plasma thermal energy, and we determine these from the brightenings in soft X-rays. For the volumetric heating rate, $H$, we have

$$H = \frac{d(3N_e k T_e)}{dt} + N_e^2 \Lambda(T_e) , \quad (3)$$

in ergs cm$^{-3}$ s$^{-1}$, where $N_e$ is the electron number density (in cm$^{-3}$), $k$ is Boltzmann's constant, $T_e$ is the electron temperature (in K), and $\Lambda$ is the radiative loss function (in ergs cm$^3$ s$^{-1}$). In terms of emission measure,

$$\mathscr{E} = \int N_e^2 dV \sim N_e^2 V , \quad (4)$$

where $V$ is the emitting volume, this is

$$H \sim \frac{d}{dt}\left[3kT_e\left(\frac{\mathscr{E}}{V}\right)^{1/2}\right] + \frac{\mathscr{E}}{V}\Lambda(T_e) . \quad (5)$$

So the total heating over time $\Delta t$ is

$$E_{\rm heat} = \int H V dt \sim 3kT_e(\mathscr{E}V)^{1/2} + \mathscr{E}\chi T_e^{-1/2}\Delta t , \quad (6)$$

where we have used $\Lambda(T_e) \approx \chi T_e^{-1/2}$. For $T_e \gtrsim 10^{5.5}$, $\chi \sim 10^{-18.81}$ (Raymond & Smith 1977).

To get $\mathscr{E}$ and $T_e$ we applied the two-filter flux-ratio analysis method for SXT images (Tsuneta et al. 1991) to our data. Strictly speaking, we should compare our expression for the prominence's difference in gravitational energy over 22:30 UT to 23:30 UT with the difference in the thermal energy over the same time period. It is difficult, however, to be certain of just what the physical conditions are of the flaring plasma prior to its brightening; that is, we are not sure whether the plasma that eventually brightens has any substantial preeruption intensity. Therefore, we merely calculate the heating energy using the temperature and emission measure after the brightening begins and consider this energy to be an upper limit for the amount of heating going on in the tether-cutting region.

We used several pairs of Al.1 and AlMg filter images between 22:23:19 UT February 8 and 00:28:37 UT February 9. We used two regions for our analysis; one is that represented by box 1 in Figure 3, and a second is the western half of that same box region. This box is of approximate size $50'' \times 100''$, and if we take the line-of-sight size to be $100''$ also, we have $V \sim 10^{29}$ cm$^3$. Both choices for the analysis region along with all our choices of image pairs give similar results, $T_e = 1.3$–$2.0$ MK and $\mathscr{E} = 10^{46}$–$10^{47}$ cm$^{-3}$. These values yield heating amounts of

$$E_{\rm heat} \lesssim (10^{28}\text{–}10^{29}) + (10^{24}\text{–}10^{25})\Delta t \text{ ergs} , \quad (7)$$

where the first and second terms represent the internal and radiative energies, respectively. Using 60 minutes in equation (7), both terms are of the same order, giving

$$E_{\rm heat} \lesssim 10^{28}\text{–}10^{29} \text{ ergs} . \quad (8)$$

Thus, we find the upper limit of the amount of heating delivered to the plasma through tether cutting to be comparable to the amount of energy required for eruption of the prominence over the first hour of the prominence's rapid eruption.

We can compare this tether-cutting heating with that of the background corona by dividing expression (8) by $\Delta t$ and by the area of box 1 of Figure 3, which is about $10^{19}$ cm$^2$. This gives a heating rate of $10^5$–$10^7$ ergs cm$^{-2}$ s$^{-1}$, since $\Delta t$, the time between the onset of fast tether-cutting reconnection and the time of the brightening onset, is no more than two hours, but could be as short as perhaps about 10 minutes; we cannot confidently narrow this time range further, in part because of *Yohkoh* night between 23:10 UT and 23:50 UT. For the quiet and active Sun, Withbroe & Noyes (1977) give respective radiative loss fluxes of $10^5$ and

$5 \times 10^6$ ergs cm$^{-2}$ s$^{-1}$. Our observed maximum heating rate over the first two hours of the prominence's fast eruption could be comparable with either of these values, considering the uncertainties in our estimates of the emitting area and other factors, and given the uncertainties in the relative meaning of the term "quiet Sun" as used by Withbroe & Noyes and ourselves. Thus, the emission we see in box 1 of Figure 3*d* (which is about two hours into the fast eruption) is consistent with tether cutting occurring, even though that emission is only slightly enhanced above that of the surrounding corona. Indeed, this brightening is not easy to discern in the nondifferenced image of Figure 2*b*; this brightening only stands out when the same image is differenced and carefully scaled in Figure 3*b*.

Now we can consider what the magnitude of the tether-cutting heating would be at an earlier time in the prominence's rise. We note that expressions (2) and (8) give $E_{\rm heat}/E_{\rm prom} \approx 1$ at the end of approximately the first hour of fast eruption, where we take the inequality to be an approximate equality in expression (8). If we make the assumption that the ratio $E_{\rm heat}/E_{\rm prom}$ remains constant during the early part of the eruption, then $E_{\rm heat}$ would be lower at the earlier times, with a correspondingly lower intensity of the tether-cutting region; for the current event, this intensity could be substantially less than that of the average background coronal heating when the prominence is at significantly lower heights. This means that at early times in the fast rise phase of the prominence, tether cutting would be taking place with an even weaker soft X-ray coronal signature than in Figure 2*b* and could be undetectable.

## 5. DISCUSSION

Our prominence rises slowly ($\approx$1 km s$^{-1}$) for about six hours prior to escaping more rapidly ($\approx$10 km s$^{-1}$) later. This is similar to the case of the filament eruption studied by Sterling et al. (2001b) and Sterling & Moore (2004). Both eruptions seem to be slower-velocity versions of erupting active-region filaments (e.g., Tandberg-Hanssen, Martin, & Hansen 1980; Foley et al. 2001, 2003), in which the eruption velocities reach several hundred km s$^{-1}$. It is also similar to the trajectory of soft X-ray plasmoids seen in SXT images (e.g., Ohyama & Shibata 1997; Nitta & Akiyama 1999). This indicates that the two-part trajectory we see is not unique and also supports our hypothesis that quiet-region and active-region eruptions differ in scale but have similar driving mechanisms. Kahler et al. (1988), however, note that erupting filaments lacking abrupt transition to rapid acceleration are also common.

We found eruption-related intensity dimmings (Fig. 3, box 3) to occur nearly concurrently and at the same locations in EIT and SXT. As these two instruments are most sensitive to material emitting at differing temperatures (§ 2), concurrent dimmings in images from both instruments at overlapping locations suggest that the dimmings result from a reduction in material density rather than from a temperature change, as discussed by Zarro et al. (1999) and Harra & Sterling (2001). Gopalswamy & Thompson (2000) found similar results using two different EIT filters. For our case here, there is apparently little plasma $\gtrsim$2 MK prior to eruption, since we found temperatures from SXT filter ratios to be only about these values. If material at the location of box 3 in Figure 3 underwent heating, we would expect increased emission there in SXT after eruption, rather than the dimming we observe.

We also found that the heating due to tether-cutting reconnection is not too strong up to about two hours following eruption onset (where "eruption onset" coincides with the start of the prominence's fast-rise phase in this example), in the sense that the resulting energy rate estimates are in the range of those of the typical heating rate of the background corona, and the coronal signature of the reconnection during this period is not prominent in the nondifferenced coronal images. Under the assumption that $E_{\rm heat}/E_{\rm prom}$ remains approximately constant during the early posteruption prominence rise, the coronal signature will be even weaker closer to the onset time, since the total amount of heating applied to the plasma via the reconnection will be less. So, for example, when the prominence has risen only a few thousand kilometers, the total heat supplied by tether cutting would be about an order of magnitude smaller than its value an hour into the eruption; the intensity of the reconnection-heated plasma would be correspondingly reduced, and so the reconnection region would be swamped by the background corona in the SXT images and perhaps undetectable even in difference images. We have some lower resolution (9.″8 pixel) SXT images available with which we can check this. We find that a difference between images at 23:57 UT and 19:23 UT (both on 1999 February 8) does not show brightenings above background noise in the reconnection region, while a difference between images at 00:20 UT (1999 February 9) and 19:23 UT (1999 February 8) is similar to Figure 3*d*; the time of eruption onset is between about 22:00 UT and 22:30 UT (Fig. 4).

To summarize our findings regarding tether-cutting reconnection: we find that, for the weak eruption considered here, the intensity enhancement in the reconnection region is weak in the coronal images taken about two hours after eruption onset, with the enhancements only obvious in difference images; we expect that the enhancements would be even weaker or invisible closer to the onset time, and our lower-resolution SXT data support this. Nonetheless, subject to our assumptions, our energy calculations indicate that the observations are still consistent with (but, of course, they are not proof of) tether cutting occurring throughout the first two hours of the fast-phase eruption, even though a coronal signature may not be detectable at those early times. It also follows that a signature of any tether cutting during the prominence's preeruption slow-rise phase would be even weaker, if our energy scaling assumption still holds during that phase. Finally, we add that, although not prominent in the nondifferenced images (Figs. 1*c* and 2*b*), the respective difference images (Figs. 3*b* and 3*d* in EUV and soft X-rays, respectively) show that brightenings are definitely occurring in the expected tether-cutting region before the prominence has traveled far from the Sun (Figs. 1*b* and 1*c*), with $\Delta h \sim$ few $\times 10^4$ km.

We do not know whether our assumption of a constant energy ratio ($E_{\rm heat}/E_{\rm prom} = 1$) is correct, but this assumption implies that the amount of energy going into mass expulsion is proportional to the amount of energy going into plasma heating, and it does not seem unreasonable that this proportionality would approximately hold throughout the early stages of the eruption. Expectations for this ratio should be checked with theoretical and numerical models of the tether-cutting process.

Our case here might be extreme, since the eruption energies involved are low. Our example of another slow eruption of 1999 April 18 discussed in Sterling et al. (2001b)

and Sterling & Moore (2004) appears to be somewhat more energetic. We are not, unfortunately, able to repeat our analysis of § 4 for that event, because there are only images from one SXT filter available in the immediate posteruption phase of that event, meaning we cannot derive $T_e$ and $\mathscr{E}$ for those times. We can, however, estimate the potential energy for that event. In that event, the erupting filament is very long and has overall dimensions of about (from Fig. 1*d* of Sterling et al. 2001b or Fig. 3 of Sterling & Moore 2004) $50'' \times 50'' \times 600''$, giving a mass $M \sim 10^{15}$–$10^{16}$ g, using the same assumptions as for the prominence of this paper. That filament's posteruption velocity was about 1.5 times that of the prominence in this paper, and so the resulting gravitational energy $E_{\rm grav} = Mg\Delta h$ will be about an order of magnitude greater than that of the event in this paper over a similar time period, $\Delta t \approx 1$ hr. Without knowledge of the energy expended in heating, we cannot check the $E_{\rm heat}/E_{\rm prom}$ ratio, but we might speculate that the $E_{\rm heat}$ at early times might be an order of magnitude greater in that case than for the event of this paper. That means that soft X-ray signatures due to tether cutting should be visible shortly after the onset of fast eruption for an event similar to that 1999 April 18 event. As discussed by Sterling & Moore (2004), the coronal observations for that event are consistent with brightenings at the time of rapid filament eruption, but SXT images are not available immediately after the fast eruption's onset in that case. This does give us hope, however, that we will be able to directly test models that involve tether cutting through timing analysis using events that are somewhat more energetic than that presented in this paper.

We thank K. Yoshimura for computer assistance, T. Kosugi for in-residence support in Japan, and T. Shimizu for useful discussions. We also thank an anonymous referee for useful comments and for pointing out numerical inaccuracies in an earlier version of the manuscript. Both authors were supported by funding from NASA's Office of Space Science through the Solar Physics Supporting Research and Technology Program and the Sun-Earth Connection Guest Investigator Program. *Yohkoh* is a mission of the Institute of Space and Astronautical Sciences (Japan) with participation from the US and UK, and *SOHO* is a project of international cooperation between ESA and NASA.

## REFERENCES

Delaboudiniere, J.-P., et al. 1995, Sol. Phys., 162, 291
Foley, C. R., Harra, L. K., Culhane, J. L., & Mason, K. O. 2001, ApJ, 560, L91
Foley, C. R., Harra, L. K., Matthews, S. A., Culhane, J. L., & Kitai, R. 2003, A&A, 399, 749
Gopalswamy, N., & Thompson, B. J. 2000, J. Atmos. Sol.-Terr. Phys., 62, 1457
Harra, L. K., & Sterling, A. C. 2001, ApJ, 561, L215
———. 2003, ApJ, 587, 429
Kahler, S. W., Moore, R. L., Kane, S. R., & Zirin, H. 1988, ApJ, 328, 824
Moore, R. L., & LaBonte, B. 1980, in Proc. IAU Symp. 91, Solar and Interplanetary Dynamics, ed. M. Dryer & E. Tandberg-Hanssen (Dordrecht: Reidel), 207
Moore, R. L., Sterling, A. C., Hudson, H. S., & Lemen, J. R. 2001, ApJ, 552, 833
Nitta, N. & Akiyama, S. 1999, ApJ, 525, L57
Ohyama, M., & Shibata, K. 1997, PASJ, 49, 249
Raymond, C., & Smith, B. W. 1977, ApJS, 35, 419
Rust, D. M., et al. 1980, in Solar Flares: A Monograph from Skylab Solar Workshop II, ed. P. A. Sturrock (Boulder: Colorado Associated Univ. Press), 273
Schmahl, E., & Hildner, E. 1977, Sol. Phys., 55, 473
Sterling, A. C., & Moore, R. L. 2004, ApJ, in press
Sterling, A. C., Moore, R. L., Qiu, J., & Wang, H. 2001a, ApJ, 561, 1116
Sterling, A. C., Moore, R. L., & Thompson, B. J. 2001b, ApJ, 561, L219
Sturrock, P. A. 1989, Sol. Phys., 121, 387
Tandberg-Hanssen, E., Martin, S. F., & Hansen, R. T. 1980, Sol. Phys., 65, 357
Tsuneta, S., et al. 1991, Sol. Phys., 136, 37
Wills-Davey, M. J., & Thompson, B. J. 1999, Sol. Phys., 190, 467
Withbroe, G. L., & Noyes, R. W. 1977, ARA&A, 15, 363
Zarro, D. M., Sterling, A. C., Thompson, B. J., Hudson, H. S., & Nitta, N. 1999, ApJ, 520, L139
Zirin, H. 1988, Astrophysics of the Sun (Cambridge: Cambridge Univ. Press)